Modeling RHEED intensity oscillations in multilayer epitaxy: Determination of the Ehrlich-Schwoebel barrier in Ge(001) homoepitaxy

Byungha Shin and Michael J. Aziz
Harvard School of Engineering and Applied Sciences, Cambridge, Massachusetts 02138, USA
(Received 9 February 2007; revised manuscript received 19 June 2007; published 8 October 2007)

We report the study of submonolayer growth of Ge(001) homoepitaxy by molecular beam epitaxy at low temperatures, 100–150 °C, using reflection high energy electron diffraction (RHEED) intensity oscillations obtained for a range of low incidence angles, where the influence of the dynamical nature of electron scattering such as the Kikuchi features is minimized. We develop a model for the RHEED specular intensity in multilayer growth that includes the diffuse scattering off surface steps and the layer interference between terraces of different heights using the kinematic approximation. The model describes the measured RHEED intensity oscillations very well for the entire range of incidence angles studied. We show that the first intensity minimum occurs well above 0.5 ML (monolayer) of the total deposited coverage, which contradicts the common practice of assigning the intensity minimum to 0.5 ML. By using the model to interpret the measured RHEED intensity, we find the evolution of the coverage of the first 1–2 ML. We find that second-layer nucleation takes place at low coverage, 0.3 ML, implying a substantial Ehrlich-Schwoebel (ES) barrier. The value inferred for the ES barrier height, 0.084±0.019 eV, includes an analysis of the beam steering effect by step edges. Comparison is made with the value of the barrier height inferred from other measurements. The model for RHEED intensity and the method of inferring the ES barrier height can be applied to any system for which RHEED measurements can be obtained without interference from Kikuchi features.

DOI: 10.1103/PhysRevB.76.165408 PACS number(s): 61.14.Hg, 68.55.−a, 81.15.Hi, 68.47.Fg

I. INTRODUCTION

Reflection high energy electron diffraction (RHEED) has become an indispensable technique in thin film growth due to its high surface sensitivity and its compatibility with growth systems such as molecular beam epitaxy (MBE).[1] Particularly, the observation of the intensity oscillation of a specularly reflected spot during growth, since it was first reported in the early 1980s,[2] is routinely used in measuring the deposition rate and determining the film growth mode. The RHEED intensity oscillation contains morphological information of the growth surface and a great deal of film growth kinetics can be learned if it is properly interpreted. However, there are still issues on which no consensus has been reached in the interpretation of RHEED intensity oscillations such as the origin of oscillations.[3,4] Approaches to this problem typically involve two parts: identification of structural parameters representing the periodic change of the growth surface exhibiting RHEED intensity oscillations and the linkage between the structural parameters and the intensity of the diffracted electron beams.

In the kinematic approximation, the oscillating coverage of a growing layer is the structural parameter and the interference of electron beams reflected off terraces of different heights is reasoned to cause the RHEED intensity oscillations.[5,6] In contrast, in the phenomenological step-density model,[7–9] RHEED intensity is reduced by the diffuse scattering off step edges whose density is, in general, believed to oscillate as long as the growth proceeds in a layer-by-layer fashion. Dynamical diffraction theories[4,10] have been proposed as alternatives to these earlier models because both of the early models are unable to explain the phase shift phenomenon[11] in which the phase of the oscillations varies with incidence angle. In the dynamical diffraction theories for intensity oscillations and the phase shift phenomenon, the main part of the scattering potential of a growing layer is assumed to vary linearly with the coverage. This causes a periodic change in the refraction conditions for electrons entering the growing layer, which affects their reflection from the bottom boundary of the growing layer.[1,4,10]

Previously, we have demonstrated that the phase shift is caused by the overlap of the specular spot and the Kikuchi features, contradicting models involving dynamical scattering theory for the phase shift.[12] At sufficiently low incidence angles, with the beam azimuth sufficiently far from a crystallographic symmetry axis, the phase shift vanishes due to the absence of the Kikuchi features. Under these conditions, RHEED intensity can be interpreted with a rather simple model without invoking complex dynamical diffraction calculations.

Our model for the RHEED specular spot intensity, which we present here, includes both the diffuse scattering off surface steps and a kinematic treatment of the layer interference between terraces of different heights. We apply the model to measured RHEED intensity oscillations for various incidence angles during homoepitaxial growth of Ge(001) by MBE at low temperatures (100–150 °C). We find that the model describes the measured RHEED intensity oscillations very well for the entire range of incidence angles used in this work. The model provides a quantitative interpretation in terms of the periodic evolution of layer coverage and step density.

In homoepitaxial film growth by MBE, there exists a well-known growth instability leading to mound formation due to an additional kinetic barrier for adatom transport downward across a step edge, the so-called Ehrlich-Schwoebel (ES) barrier.[13,14] Experimental evidence of an instability induced by the ES barrier during MBE growth has

been reported in many semiconductor materials including Si,[15] Ge,[16,17] and GaAs,[18] as well as in metals.[19–21] The ES barrier controls the rate of interlayer mass transport and is an important kinetic parameter in determining the evolution of homoepitaxial growth.

Several methods have been proposed to estimate the magnitude of the ES barrier from experimental data.[14,16,20–35] One of these approaches involves the onset of second-layer nucleation on top of islands when they have reached a critical size.[22–24,27] This critical size decreases with increasing adatom supersaturation on top of the island, which increases with increasing ES barrier height.[22,25,27] Another approach focuses on the evolution of the individual layers of a structure with several exposed layers.[21,24,29,33] The ES barrier determines the relative distribution of deposited adatoms into islands on the same layer, where the flux is incident, and into the islands one level below by crossing the descending steps. Hence, by monitoring the growth rate of each layer, one can infer the magnitude of the ES barrier. Most cases of applying these methods to experimental results have relied on real-space imaging techniques such as scanning tunneling microscopy (STM),[16,20] atomic force microscopy (AFM),[16] or low-energy electron microscopy.[21,29] Kinetic Monte Carlo (KMC) simulations have been also used in estimating the magnitude of the ES barrier as that resulting in the best agreement between the RHEED intensity from KMC simulations and the measured RHEED intensity.[30,31] However, the RHEED intensity is assumed to be fully describable solely either by the kinematic approximations[31] or by the step-density model.[30] Here, we use our model describing RHEED intensity to interpret our RHEED intensity oscillation measurements in the submonolayer[36] growth in Ge(001) homoepitaxy; the result is an inferred ES barrier height of 0.084 ± 0.019 eV.

The paper is organized as follows. We present the experiments in Sec. II. Section III describes the model for RHEED intensity and its application to the measured intensity oscillations to infer the evolution of individual layer coverage. In Sec. IV, we infer the ES barrier height for Ge(001). We present a discussion and conclusions in Secs. V and VI, respectively.

II. EXPERIMENTS

An electron beam of 15 keV is employed for the RHEED measurements. RHEED patterns imaged on a phosphor screen are transferred by a charge coupled device camera with a temporal resolution of 1/30 s into a commercially available software package[37] for data collection and analysis. All the data presented in this paper are obtained from Ge(001) homoepitaxy by MBE at 100 and 150 °C. The details of substrate preparation and MBE growth are reported elsewhere.[38] The incidence angle of the electron beam ranges from 0.35° to 0.64° from grazing. Azimuthally, the electron beam is directed 7° off from ⟨110⟩.[12] Prior to every intensity oscillation measurement, a buffer layer of 50 nm is grown at 370 °C to provide a smooth starting surface. AFM reveals that the starting surface consists of terraces of an average size of ~150 nm separated by steps running along ⟨100⟩.

Figure 1 shows the RHEED intensity oscillations collected for 40 s of MBE growth of Ge(001) at 150 °C with incidence angles ranging from 0.35° to 0.64° at an azimuthal orientation of 7° off ⟨110⟩. These conditions are chosen so that no phase shift of the intensity oscillations is observed. Under these conditions, the specular beam is not affected by the Kikuchi features, which has been identified as the origin of the phase shift of the intensity oscillations from our earlier work.[12] Hence, the current geometry minimizes the dynamical scattering nature of electron diffraction. In all oscillations shown in Fig. 1, the period of the first oscillation is smaller than the subsequent ones by almost 30%, which is due to a transient high flux immediately after opening the shutter of the effusion cell containing MBE source materials.[12] The bottom curve of Fig. 1 is slightly out of phase with the others because of a drift of the deposition flux from run to run. The most striking feature apparent in Fig. 1 is the reduction of the overall RHEED intensity with increasing incidence angle. One can understand this change in the intensity qualitatively using the kinematic approximation. For Ge(001) surfaces with an incident electron beam of 15 kV, the incidence angle fulfilling the out-of-phase condition, where the complete destructive interference between electrons reflected from terraces of different levels is realized, is 0.99°. As the diffraction condition approaches the out-of-phase condition, i.e., with incidence angle increasing toward 0.99°, the interference becomes gradually more destructive, thereby reducing the RHEED intensity. However, the rate of the intensity drop over the change in the incidence angle expected merely from the kinematic approximation is larger than what we observe.

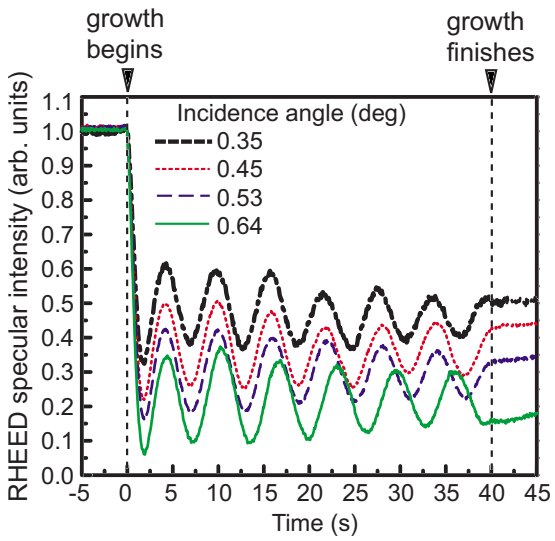

FIG. 1. (Color online) RHEED specular intensity oscillations collected at various incidence angles during MBE growth at 150 °C. Growth begins at 0 s on the time axis and finishes at 40 s. RHEED beam azimuth is 7° off the ⟨110⟩ direction. Buffer layer of ~50 nm was grown at 370 °C between successive RHEED oscillation measurements providing same smooth starting surface.

III. MODEL FOR REFLECTION HIGH ENERGY ELECTRON DIFFRACTION SPECULAR INTENSITY

Two major models used in describing the RHEED specular intensity are the kinematic approximation and the phe-

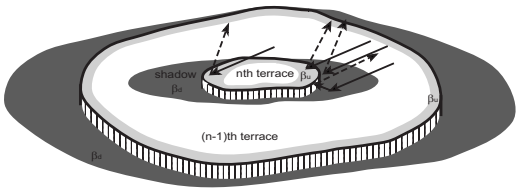

FIG. 2. Illustration of diffuse scattering off step edges. White parts of terraces give ideal kinematic diffraction. Incoming electrons (solid arrow lines) arriving at gray bands are nonspecularly scattered (dashed arrow lines) off step edges. The characteristic widths of light and dark gray bands are β_u and β_d, respectively.

nomenological step-density model. Both models explain some aspects of RHEED intensity oscillations. For example, the kinematic approximation has been evoked to explain the dependence of the amplitude of the intensity oscillations on incidence angle.[6] The observation of intensity oscillations at the in-phase diffraction condition has been used as evidence supporting the step-density model.[8,39] It is our view that in actual film growth, the main diffraction processes assumed in the kinematic approximation and in the step-density model are both responsible for the RHEED intensity variation. Therefore, we have developed a model to describe the RHEED specular intensity combining both the diffuse scattering from step edges and the layer interference in the kinematic approximation.

We propose the following expression for the specular RHEED intensity I normalized by the predeposition value I_0:

$$I/I_0 = \Big| [1-\beta_u S(\theta_m)]\theta_m \exp(iq_z md) + \sum_{n=2}^{m} \{[1-\beta_d S(\theta_n) - \beta_u S(\theta_{n-1})](\theta_{n-1}-\theta_n)\exp[iq_z(n-1)d]\} + [1-\beta_d S(\theta_1)](1-\theta_1)\Big|^2, \quad (1)$$

where m is the total number of incomplete layers of a growth front, θ_n is the individual layer coverage (hence $\theta_n - \theta_{n+1}$ is the exposed layer coverage of the nth layer), d is the interlayer spacing perpendicular to the surface, and q_z is the wave number corresponding to momentum transfer along the surface normal. q_z is dependent on the incidence angle via $q_z = 4\pi \sin \alpha_{inc}/\lambda$, where α_{inc} is the incidence angle and λ is the incident electron wavelength. β_u and β_d are the characteristic lengths of electron scattering by step edges that reduce the electron flux that otherwise diffracts kinematically from the upper terrace and lower terrace, respectively. Figure 2 depicts diffuse scattering of incident electrons by the step edges bounding the nth and $(n-1)$th layer islands; incoming electrons (solid arrow lines) arriving at the gray bands are nonspecularly scattered (dashed arrow lines) by the step edges. The width of the light and the dark gray bands represent β_u and β_d, respectively. The local scattering strength may vary depending on the relative orientation of a step segment with respect to the incident electron beam, as indicated schematically by the varying thickness of the gray bands around the islands in Fig. 2. Therefore, β_u and β_d in our model should be considered as average values over all step segments. The model assumes that a part of the total electron flux incident upon a sample is scattered off step edges and the remaining flux participates in the layer interference within the kinematic approximation; the first factor in each term of Eq. (1) is responsible for the loss of electron flux due to the step edges. The first term in Eq. (1) represents the contribution of the top layer, i.e., the mth layer, to the RHEED intensity; hence, only β_u appears in that term. Likewise, for the bottom layer, only β_d appears in the third term of Eq. (1). Korte and Maksym[40] claimed from their dynamical calculations that increasing the step density at a fixed coverage tends to increase the specularly reflected RHEED intensity in contrast to the phenomenological step-density model. However, as pointed out by Bell *et al.*,[41] the concept of a disordered growing layer employed in the dynamical diffraction calculations by Korte and Maksym may not be relevant here as the Ge(001) surface rearranges itself very rapidly into the well ordered (2×1) reconstruction.[42] Furthermore, there has been experimental work[8,9] supporting the anticorrelation between the RHEED specular intensity and the surface step density, which is the essential idea behind the step-density model. We adopt the conventional view of the role of the step edge as a scattering center reducing the specular intensity; hence, the β's in our model are restricted to positive values.

In a typical RHEED geometry of near-grazing incidence, a significant shadowing effect[43] is anticipated. There exists a shadowed region on a terrace from steps to the terrace immediately above, where grazing-incidence electrons are not able to reach and diffract kinematically, as illustrated in Fig. 2. In this geometry, this shadowing effect is likely to be dominant over other possible mechanisms responsible for the loss of electron flux. Hence, we assume that $\beta_d \gg \beta_u$ and Eq. (1) can be approximated as

$$I/I_0 = \Big| \theta_m \exp(iq_z md) + \sum_{n=2}^{m} \{[1-\beta S(\theta_n)](\theta_{n-1}-\theta_n) \times \exp[iq_z(n-1)d]\} + [1-\beta S(\theta_1)](1-\theta_1)\Big|^2, \quad (2)$$

where $\beta \equiv \beta_u$.

For a "one-layer system," $m=1$, two distinct layers contribute to diffraction and Eq. (2) reduces to

$$I/I_0 = \theta_1^2 + [1-\beta S(\theta_1)]^2(1-\theta_1)^2 + 2[1-\beta S(\theta_1)] \times \theta_1(1-\theta_1)\cos(q_z d). \quad (3)$$

This is the same as Eq. (19.14) of Ichimiya and Cohen,[1] which was developed explicitly for the one-layer system. Hence, our model [Eq. (1)] can be considered as an extension of that of Ichimiya and Cohen to multiple layers and to nonzero β_u.

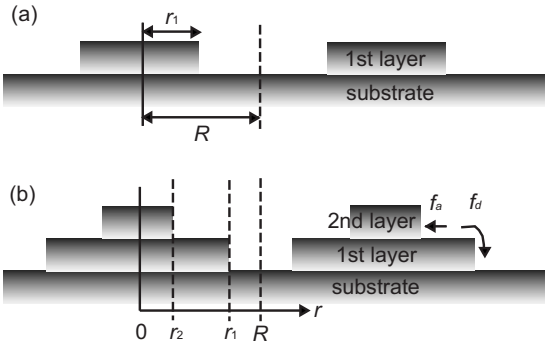

FIG. 3. Schematic showing island structure assumed in our treatments for (a) one-layer regime and (b) two-layer regime. First-layer islands are uniformly spaced with distance $2R$ and second-layer islands nucleate at the center of first-layer islands. f_a and f_d denote flux (per unit length of step) attached to second-layer islands and attached to first-layer islands after crossing descending steps, respectively.

To apply our model to the measured RHEED intensity oscillations, first we need to know the density of islands on the growing surface and their shape so as to quantify step density $S(\theta)$. A vast body of work has been performed on the subject of the nucleation and growth of islands during thin film growth. Most studies have demonstrated that upon beginning growth, the adatom density builds up and, once it exceeds a critical value, islands start to nucleate. Subsequently, the adatom density decreases and the number of islands increases until saturation. In the saturation regime, islands grow and the nucleation of new islands hardly occurs. Finally, when islands become large, they start to coalesce, reducing the island density. The duration of the saturation regime and the onset of coalescence are influenced by growth conditions. However, it is well accepted that the transition to the saturation regime occurs at the very early stage under most growth conditions.[44–47] For a ratio of diffusivity to deposition flux $D/a^4F \sim 10^5$ (where the diffusivity D is in $\mathrm{cm}^2\ \mathrm{s}^{-1}$, the flux F is in $\mathrm{cm}^{-2}\ \mathrm{s}^{-1}$, and a is the lattice spacing) which is close to our experimental conditions, the transition happens as early as 0.001 ML (monolayer) of deposition.[44] Here, in our model for the surface morphology, a saturation island density is assumed from the very beginning of growth, so we are slightly overestimating the step density but only for the first few data points in the RHEED intensity spectra because of the early transition into the saturation regime. We also assume that the surface is composed of identically sized circular islands that are regularly spaced with a spacing $2R$, as shown in Fig. 3(a). Coalescence of islands is not considered, resulting in the overestimation of the step density at higher coverages where one expects some degree of island coalescence. With these assumptions, until the second-layer nucleation occurs, the step density of the first-layer islands, $S(\theta_1)$, is expressed as follows:

$$S(\theta_1) = N2\pi r_1 = \frac{g}{R}\sqrt{\theta_1}, \tag{4}$$

where N denotes the steady-state island density which is a constant and g is a geometric factor, which is $(4\pi/3\sqrt{3})^{1/2}$ for a hexagonal array of islands. Combining Eqs. (3) and (4), the RHEED specular intensity before the nucleation of the second layer is

$$I/I_0 = \theta_1^2 + \left(1 - \frac{g\beta}{R}\sqrt{\theta_1}\right)^2 (1-\theta_1)^2 + 2\left(1 - \frac{g\beta}{R}\sqrt{\theta_1}\right) \times \theta_1(1-\theta_1)\cos(q_z d). \tag{5}$$

We use this expression for fitting the earliest portion of the measured RHEED intensity, in Fig. 4, up to 0.3 ML, a limit which will be justified subsequently. There is only one fitting parameter in Eq. (5), which is β/R. Following common practice, we make an initial mapping (to be revisited later) of growth time onto coverage such that the first intensity minimum and maximum occur at a 1/2 ML and 1 ML of coverage, respectively. The model fits only up to a certain coverage in each case; beyond that coverage, the intensity from our model is well above the measured value. The divergence suggests the roughening of the surface beyond an one-layer system, i.e., the onset of second-layer nucleation.

For a two-layer system, as shown in Fig. 3(b), the model for the intensity becomes

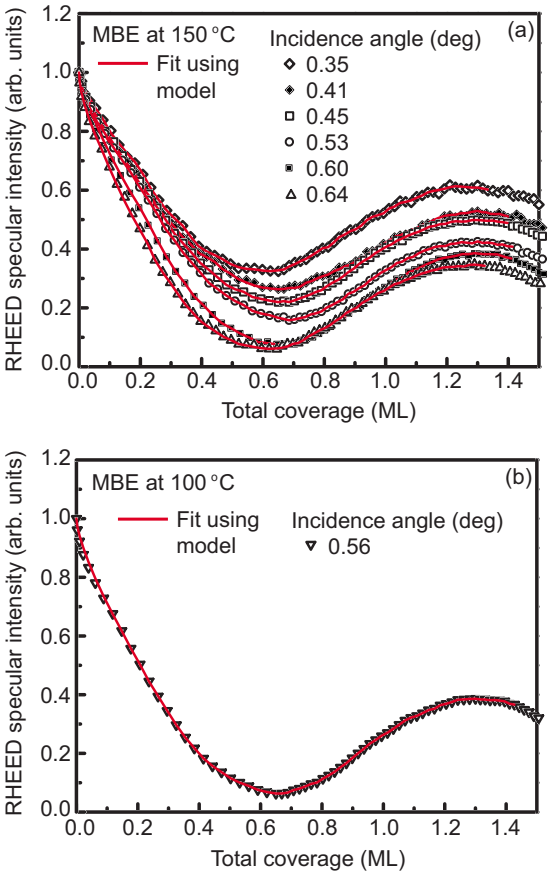

FIG. 4. (Color online) RHEED specular intensity oscillations collected at (a) 150 °C for various incidence angles and (b) at 100 °C with incidence angle of 0.56°. Line drawn on top of measured RHEED intensity oscillations is fit using the model.

$$I/I_0 = \left(1 - \frac{g\beta}{R}\sqrt{\theta_1}\right)^2 (1-\theta_1)^2 + \left(1 - \frac{g\beta}{R}\sqrt{\theta_2}\right)^2 (\theta_1-\theta_2)^2 + \theta_2^2 + 2\left(1 - \frac{g\beta}{R}\sqrt{\theta_2}\right)(\theta_1-\theta_2)\left[\theta_2 + \left(1 - \frac{g\beta}{R}\sqrt{\theta_1}\right)(1-\theta_1)\right] \times \cos(q_z d) + 2\left(1 - \frac{g\beta}{R}\sqrt{\theta_1}\right)(1-\theta_1)\theta_2 \cos(2q_z d). \quad (6)$$

We introduce the ratio of θ_2 to θ_1, k, which is the only unknown for a given total coverage $\theta = \theta_1 + \theta_2$, as the value of $g\beta/R$ is available from the fitting of the model to the earlier one-layer regime. Now, we can find the value of k that allows the intensity from Eq. (6) to match the measured intensity. Because, however, for a two-layer system the intensity minimum may not occur at 1/2 ML of total deposition, we revisit the mapping of growth time to total coverage. For values for k in the range 0.1–0.5, we find from Eq. (6) the total coverage giving rise to the first minimum of the intensity and observe that with increasing k (i.e., increasing fraction of the second-layer islands), the coverage of the first intensity minimum $\theta_{\min}$ increases beyond 1/2 ML. Thus, we search for a pair of values for k and $\theta_{\min}$ that permits the first minimum of Eq. (6) to be equal to that of the measured RHEED intensity. For all incidence angles studied, we find that k lies between 0.3 and 0.4 and $\theta_{\min}$ is near 0.65 ML, which is 1.3 times the originally assumed intensity-minimizing coverage of 0.5 ML. The significance of this finding is that unless the intensity maxima recover to the predeposition value (i.e., perfect one-layer growth), the coverages of the intensity minima differ from half-integer values and the discrepancy can be large for a well-developed multilayer growth.

Having a more refined mapping of growth time to coverage, we revisit the earlier part of growth, the one-layer regime, and reevaluate $g\beta/R$. Using this reevaluated value, we repeat the search of $\theta_{\min}$ and $k(\theta_{\min})$ that makes the measured intensity minimum equal to the value expected from Eq. (6). We iterate the reevaluation of $g\beta/R$ and $\theta_{\min}$ to convergence. With the converged β/R and $\theta_{\min}$, fitting of the two-layer regime is achieved by allowing $k(\theta)$ to vary from one data point to the next. Beyond $\theta \sim 1.15$ ML,[48] the third-layer nucleation has to be also considered in order to match the intensity from the model and the measured intensity. Because we neglect coalescence in the treatment, as soon as the first layer reaches completion in the model, there is a discontinuous drop in the step density, which is artificial. For this reason, fitting the model to the data beyond $\theta_1 \sim 1$ ML ($\theta = 1.35$ ML for $k \sim 0.35$) is not carried out. In reality, the contribution of the first layer to the total step density decreases gradually as the coalescence progresses.

The results of the model are superposed on the measured RHEED intensity curves in Figs. 4(a) and 4(b). As $g\beta/R$ is obtained from the fitting, in order to evaluate β for the growth at 100 and 150 °C, the average island spacing R from both temperatures has to be known. Li and Altman[49] investigated submonolayer growth of Ge(001) using STM and found that Ge islands on the (2×1) reconstructed (001) surfaces exhibit an anisotropic shape. At 150 °C and 0.2 ML of deposition, the average island spacings are 5.4 and 11.0 nm for the substrate $1\times$ direction (along the substrate dimer rows) and $2\times$ direction (perpendicular to the substrate dimer rows), respectively. We take the average of both directions as the island spacing at 150 °C under the growth condition used by Li and Altman at that temperature.[49] To account for the different deposition rates (and growth temperature for our data obtained at 100 °C), we employ the well-known scaling relationship from the two-dimensional (2D) nucleation theory,[50] $N \sim (D/F)^{-\chi}$, where N is a steady-state island density. The exponent χ becomes 1/3 when the smallest stable nucleus consists of two mobile entities on the surface. The mobile building unit of the Ge(001) surfaces has been shown to be an ad-dimer rather than an adatom,[51,52] and D in this paper, unless specified otherwise, represents the diffusivity of the ad-dimers. The value of the activation barrier of ad-dimer diffusion used in our analysis is ~0.82 eV, which is the barrier of diffusion along the underlying dimer rows, known as the fastest diffusion path as measured by Afanasieva *et al.*[51] We choose the average island spacing of the submonolayer growth regime as 5.3 nm at 150 °C and 3.6 nm at 100 °C. Using these island spacings, the characteristic lengths of electron scattering by step edges, β from the 150 °C results is determined to vary between 0.83 and 0.87 nm for different incidence angles. However, β does not exhibit any systematic dependence on the incidence angle. The variance in β for different incidence angles at 150 °C here must be from experimental fluctuations. β from the 100 °C result is 0.75 nm, which is close to the values for 150 °C.

Figure 5(a) shows the evolution of the individual layer coverage extracted from the RHEED results from the growth at 150 °C for various incidence angles, 0.35°–0.64°, using the model described in the previous section. Note that statistically identical surface evolution is monitored by RHEED with different incidence angles on different (but nominally identical) growth runs. Figure 5(a) shows that the results of the model applied to different RHEED geometries on different runs are indistinguishable, providing a consistency check for the validity of our model for the RHEED intensity. In the model, the only fitting parameter for the one-layer regime is β/R, which is used without modification as an input to the model for the two-layer regime. Within the two-layer regime, $k(\theta_{\min})$ is treated as a fitting parameter. With these values of β/R and $k(\theta_{\min})$, the model then determines $k(\theta)$ at every data point required to match the measured intensity in the two-layer regime.

As our model essentially relates the structural parameters of step density and layer coverage to the RHEED specular intensity, continuous evolution of those quantities during growth is available from the RHEED measurements. The real-time nature of this information provides a valuable complement to postgrowth real-space imaging. The model should be applicable to any system in which RHEED measurements are possible away from Kikuchi features.

In the next section, we inferred growth kinetic parameters, in particular, the ES barrier using the evolution of individual layer coverages obtained from the RHEED intensity oscillations.

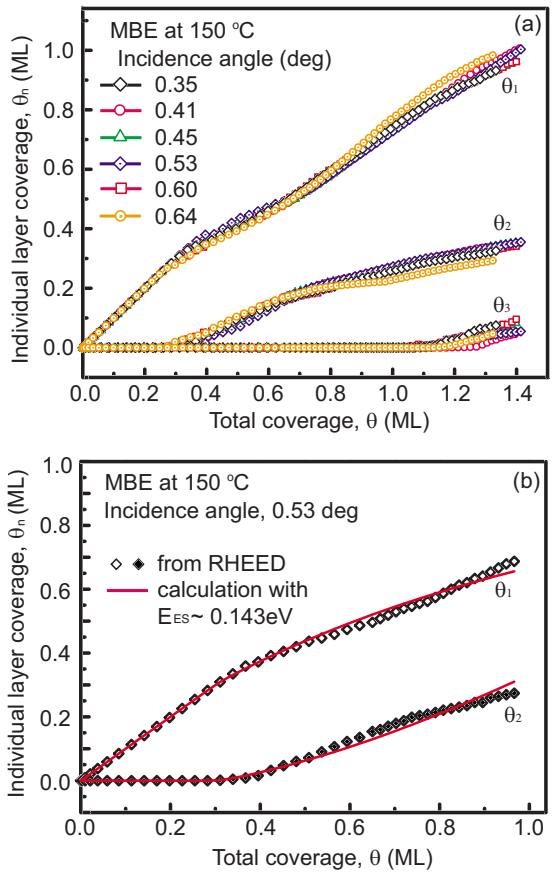

FIG. 5. (Color online) (a) Plot of evolving individual layer coverage extracted from RHEED intensity variations for various incidence angles during MBE at 150 °C. θ_1, θ_2, and θ_3 represent first-, second-, and third-layer coverages, respectively. (b) Evolution of layer coverages for incidence angle of 0.53° [also shown in (a)] with calculated layer coverage with ES barrier of ~0.143 eV shown as solid lines.

IV. DETERMINATION OF THE EHRLICH-SCHWOEBEL BARRIER

It is noticeable from Fig. 5(a) that for Ge(001) homoepitaxy at 150 °C, the second-layer nucleation takes place as early as ~0.3 ML, suggesting a substantial ES barrier preventing interlayer mass transports. In examining the effect of the ES barrier on the growth mode, Tersoff *et al.*[22] introduced the concept of the critical island size (radius in the case of circular islands), R_c for the second-layer nucleation. The treatment begins with evaluating the nucleation rate (per unit area) ω and the total nucleation rate Ω on top of an island with radius R by integrating ω over the entire area of the island. Once Ω is known, the fraction f of islands with a second layer nucleated on top increases over time following $df/dt=\Omega(1-f)$, the solution of which is

$$f = 1 - \exp[(-R/R_c)^m], \tag{7}$$

where the exponent m depends on the ES barrier height and the size of the smallest stable nucleus.[22] The fraction given by Eq. (7) sharply increases as the size of islands approaches the critical size R_c. In evaluating ω (and Ω), Tersoff *et al.*[22] used the 2D nucleation theory, where the nucleation rate is derived from rate equations describing the atomic processes such as adatom attachment to and detachment from clusters with the assumption of a constant capture number, i.e., the mean-field approximations.[50]

This mean-field approach, however, has been criticized by several researchers.[27,28,53,54] Rottler and Maass[53] demonstrated in their KMC simulations different scaling properties of R_c from those of Tersoff *et al.* The scaling relationship of R_c found by Rottler and Maass[53] has been confirmed by succeeding theoretical studies that take into account of the strong fluctuations of the actual adatom concentration on the islands as opposed to the time-averaged value used in the mean-field approach.[27,28,54] The main argument against the mean-field approach is that it overestimates the nucleation rate on top of confined geometries; therefore, the comparison of R_c derived by Tersoff *et al.*[22] with experimentally measured R_c would lead to the underestimation of the ES barrier.[27,28,54] It was shown by Politi and Castellano[54] that the mean-field approach to nucleation overestimates the nucleation rate. In the subsequent work,[55] they undertook an exact computation of the nucleation rate which can be, in principle, translated into R_c by means of numerical methods. However, in some limiting cases defined by comparing relevant time scales, simple analytical expressions of R_c are available.

Another approach for estimating the ES barrier, similar to identifying R_c just described above, is through the concept of critical adatom density[23,24]—when the adatom density exceeds this critical value, the nucleation of new islands occurs. This approach assumes that the critical adatom densities for nucleation *on a substrate* ρ_{0c} and on *a first-layer island* ρ_{1c} are the same. One can obtain ρ_{c0} from the density of first-layer islands on the substrate. The spatial distribution of adatoms on the first-layer island ρ_1 is given by solving the diffusion equation with the ES barrier incorporated into the boundary conditions. The maximum adatom density on the first-layer island is the value of ρ_1 evaluated at the center of the island. From the assumption of the same critical density for nucleation on both the substrate and the first-layer island, the ES barrier is determined by equating ρ_{0c} and the maximum value of ρ_1. However, this assumption has been questioned and it was shown that ρ_{1c} can be much larger than ρ_{0c} in the case of the strong ES barrier.[25,27]

As an alternative approach to focusing on the onset of second-layer nucleation, evolution of individual layers following the second-layer nucleation has been used to infer the ES barrier.[21,24,29,33] The distribution of the 2D flux arising from deposition onto a terrace enclosed by two steps (one ascending and one descending step) is determined by the strength of the ES barrier. When there is no ES barrier and the difference in the chemical potential at the step edges that could be induced either by step-step interactions or step curvature is ignored, half of the flux (per unit length of step) attaches to the ascending step and the other half traverses the descending step. Any finite barrier disturbs the equal distribution and, therefore, controls the relative growth rate of the coverages of different levels.

TABLE I. List of estimated ES barriers for different conditions of growth and RHEED measurements. Columns 3–5 show ES barriers extracted by the method described in Secs. IV A and IV B for different strengths of beam steering effect. Last column lists ES barrier estimated using Eq. (11) and R_c (shown in column 6) determined from the analysis of RHEED results.

Conditions for RHEED measurements		ES barrier with different steering strengths (eV)				
Incidence angle (deg)	Growth temp. (°C)	Steering strength: 0	Steering strength: 0.2 nm	Steering strength: 0.4 nm	R_c from RHEED (nm)	ES barrier using Eq. (11) (eV)
0.35	150	0.109	0.085	0.064	2.34	0.095
0.41	150	0.132	0.103	0.081	2.66	0.062
0.45	150	0.116	0.090	0.078	2.58	0.070
0.53	150	0.143	0.110	0.084	2.54	0.074
0.60	150	0.105	0.083	0.063	2.88	0.042
0.64	150	0.083	0.062	0.041	2.47	0.081
0.56	100	0.089	0.056	0.046	1.78	0.024
Average		0.111±0.021	0.084±0.019	0.065±0.017		0.064±0.024

A. Determination of the Ehrlich-Schwoebel barrier using the evolution of individual layers

The relative distribution of flux attaching to a unit length of ascending step, f_a, and traversing a unit length of descending step, f_d [see Fig. 3(b)], can be determined by solving the diffusion equation described below. Using the quasistationary approximation,[23–26,29] the excess adatom concentration ρ in the second layer on the terrace of a first-layer island is described by

$$\partial\rho/\partial t = D\nabla^2\rho + F \approx 0. \tag{8}$$

The boundary conditions involved in Eq. (8) are

$$f_a = a\rho(r_2)\nu\exp\left(-\frac{E_D}{k_BT}\right) = D\left.\frac{d\rho}{dr}\right|_{r=r_2},$$

$$f_d = a\rho(r_1)\nu\exp\left(-\frac{E_D+E_{ES}}{k_BT}\right) = D\left.\frac{d\rho}{dr}\right|_{r=r_1},$$

where E_D is the diffusion barrier for ad-dimer hopping on the terrace, E_{ES} is the ES barrier, a is the hopping distance of ad-dimers,[56] ν is an effective attempt frequency[57] to cross over downward steps, $D=(a^2/4)\nu\exp(-E_D/k_BT)$, and k_BT has the conventional meaning.[58] $\rho(r_2)$ and $\rho(r_1)$ denote the ad-dimer concentration in the second layer in the immediate vicinity of the ascending steps and the descending steps, respectively.[33] The solution of Eq. (8) with 2D axial symmetry is given by $\rho(r)=A+B\ln r-(r^2/4)(F/D)$.[23] By applying the boundary conditions, the constants A and B are obtained as follows:

$$B = \frac{(F/D)(r_1^2/4 - r_2^2/4 + ar_1/2\alpha + ar_2/2)}{a/\alpha r_1 + a/r_2 + \ln(r_1/r_2)},$$

$$A = B(-a/\alpha r_1 - \ln r_1) + (F/D)(r_1^2/4ar_1/2\alpha),$$

where $\alpha \equiv \exp(-E_{ES}/k_BT)$. In solving for the constants A and B, the attempt frequencies for the hopping on the terrace and over the descending steps are assumed to be the same.[21,30,59] The ratio p of the total current outward into the first-layer islands to that inward into the second-layer islands is

$$p = \frac{2\pi r_1 f_d}{2\pi r_2 f_a} = \left(-B + \frac{r_1^2}{2}\frac{F}{D}\right) \Big/ \left(B - \frac{r_2^2}{2}\frac{F}{D}\right). \tag{9}$$

Until the third-layer islands nucleate, the entire current incident on top of the second-layer islands is expected to traverse the descending steps onto the first layer, contributing to the growth of the second-layer islands. The growth rate of the first-layer islands is determined by the sum of the flux landing on the substrate level and the part, $p/(p+1)$, of the current deposited on the first-layer islands that makes it to the substrate. All the quantities required to determine the growth rate of individual layer coverages are thus known except α, which is related to the ES barrier height and which is to be used as a fitting parameter. Figure 5(b) shows one of the curves from Fig. 5(a) with the calculated evolution using the ES barrier height that offers the best fit. Fits for all data sets result in inferred ES barrier heights listed in Table I.

B. Effect of the beam steering

Depositing atoms experience an attractive potential as they arrive in the vicinity of the substrate, causing a deflection of their trajectories.[60] This steering effect bears no significant consequence in terms of the uniformity of the deposition flux on an atomically flat surface. However, any atomic-scale features on the surface such as islands can disturb the uniformity of the flux and the consequence was demonstrated to be pronounced especially in grazing incident

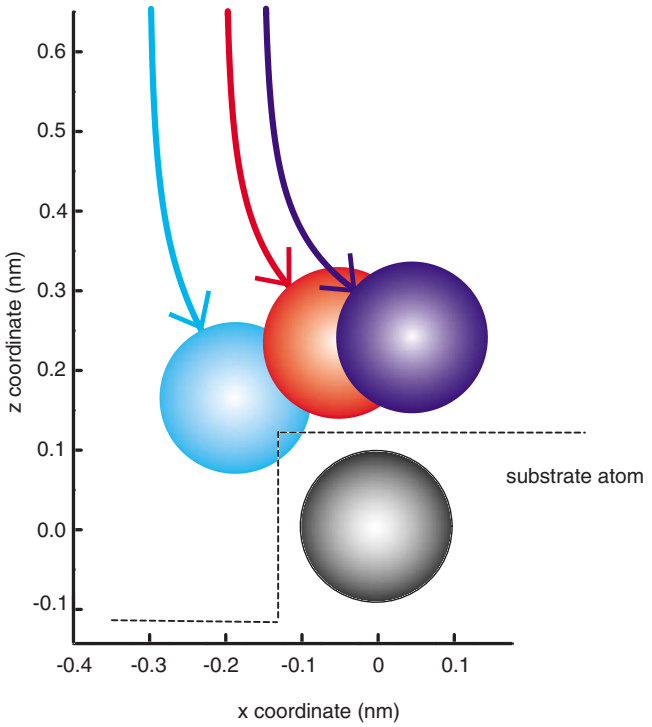

FIG. 6. (Color online) Calculated trajectories of depositing atoms located at different positions. Atom at (0, 0) represents the substrate atom and dotted line delineates the island. Final positions of depositing atoms are shown.

deposition.[61] The impact of the steering effect on the instability of homoepitaxial growth in connection with the ES barrier was examined by Politi and Castellano.[28] Islands on the surface tend to attract more flux than expected from uniform deposition, thus increasing the chances of nucleation of a new layer on top, which has the same effect as if the ES barrier increased. Therefore, neglecting the steering effect would lead to the overestimation of the ES barrier.

To appreciate the degree of the beam deflection during a normal deposition on the Ge(001) surface, we carry out simple atomic trajectory calculations, as shown in Fig. 6. The coordinate system is set up such that z direction represents normal to the (001) surface. A depositing atom and a substrate atom are restricted to lie in the plane of the page, $y=0$. We consider the force on the incoming atom from only the most influential substrate atom, which is located at the island edge, $(x,z)=(0,0)$. We seek to evaluate the disturbance of the flux induced by the steering effect. Incoming atoms are launched in the $-z$ direction with lateral positions $-0.3\text{nm}<x<-0.15$ nm, as shown in Fig. 6. The initial kinetic energy of the depositing atoms is set as ~0.136 eV from k_BT with T being the temperature of the effusion cell, 1300 °C. The Lennard-Jones (LJ) potential, $V(r)=4\epsilon[(\sigma/r)^{12}-(\sigma/r)^6]$, is employed in our calculations. r in the equation denotes the distance between the interacting particles. The parameters ε and σ are chosen so as to yield a correct cohesive energy and the stable atomic distance for Ge: $\varepsilon=1.93$ eV and $\sigma=0.245$ nm. The force exerted on the depositing atoms through the LJ potential is evaluated each 0.05 ps during which the depositing atoms are accelerated by a constant force. The calculations are continued until the atoms settle at the stable distance from the substrate atom, 0.245 nm. Figure 6 illustrates the trajectories of three atoms displaced laterally from the substrate atom by 0.15–0.3 nm. One can see from Fig. 6 that the incoming atoms within ~0.2 nm laterally beyond the corner atom of an island will deflect during the course of travel sufficiently to land on the island. So we estimate 0.2 nm as the strength of the steering effect in Ge homoepitaxy.[28] From this effect, the average flux on top of islands of a radius r (in nanometers) will increase by a factor of $(r+0.2\text{ nm})^2/r^2$. Now, the flux in Eq. (8) is replaced by this effective flux, and all the quantities affecting the individual layer evolution obtained by solving Eq. (8) are reevaluated accordingly. The results are given in Table I. Noticeable reduction in the estimated ES barrier by the steering effect is apparent. Further strengthening the steering effect to 0.4 nm, which does not seem to be physically achievable, nevertheless results in an additional reduction of the ES barrier, as expected. We take 0.084 ± 0.019 eV as our best estimate of the barrier height.

Politi and Castellano[28] examined the steering effect in the interpretation of the experimental data of Kalff *et al.* [34] for R_c of Pt(111) homoepitaxy with varying partial pressure of CO. They found that the estimated value of the ES barrier is affected by the steering but the influence of the steering seems rather weak. The inferred ES barrier is reduced from 0.31 to 0.28 eV in one case. It is reduced from 0.13 to 0.12 eV in another when the strength of the steering varies from 0 to unphysically very large, 32 times the lattice spacing of the Pt(111) surface.[62] In contrast, we observe a much larger effect of steering in inferring the ES barrier: a reduction by almost 20% with a steering strength of roughly 0.5 times the lattice spacing of Ge(001). This difference may arise from the differing methods to determine the ES barrier used in their work and ours. Politi and Castellano[28] determined the ES barrier from measurements[34] of the critical size R_c (the method to be discussed in the next section), which basically utilizes one snapshot of growing islands. On the other hand, we take advantage of the entire evolution of both first- and second-layer islands, which should provide a more thorough picture of the evolution.

C. Determination of Ehrlich-Schwoebel barrier using the critical size, R_c

Although the model based on the concept of the critical size developed by Tersoff *et al.*[22] has been commonly used in interpreting experimental results of mostly metal homoepitaxy and deducing the ES barrier,[20,34,35] the mean-field approach inherent in the model has been disputed by subsequent theoretical works[27,28,53,54] for the reasons explained in the early part of Sec. IV. The expressions relating the critical size for the second-layer nucleation and the ES barrier beyond the mean-field approach, which are claimed to be more precise due to more accurate calculations of the nucleation rate, are now available.[27,28,54,55] For some limiting cases, the expressions can be approximated to simple analytical formula. The boundary of these limiting cases is delineated by comparing magnitudes of three time scales during growth of

islands: the traversal time (τ_{tr}), which is the average time required for an adatom on an island to diffuse to the edges; the residence time (τ_{res}), which is the average time spent by an adatom until it jumps over the descending steps bounding the island; and the deposition time (τ_{dep}), which is the time interval between successive deposition events on the island. For a circular island of radius r, they are given as follows[54]:

$$\tau_{tr} = \frac{1}{8}\frac{r^2}{D},$$

$$\tau_{res} = \left(\frac{1}{8}r + \frac{1}{2}l_{ES}\right)\frac{r}{D},$$

$$\tau_{dep} = \frac{1}{F(\pi r^2)}, \tag{10}$$

where the ES length is defined as $l_{ES}=a[\exp(E_{ES}/kT)-1]$.[63] Under the practical growth conditions, τ_{dep} is much larger than the others. τ_{res} and τ_{tr} are related such that an adatom reaches the boundary of the island roughly τ_{res}/τ_{tr} times until it eventually jumps over the descending steps of the island. When $\tau_{tr} \ll \tau_{res} \ll \tau_{dep}$, it is categorized as the strong ES barrier regime. For zero or weak ES barriers, $\tau_{tr} \approx \tau_{res} \ll \tau_{dep}$.

For the strong ES regime and circular island geometry, Krug *et al.*[27] derived the following equation:

$$R_c = \frac{1}{2\pi}\left[\frac{7(2\pi)^4}{2}\frac{a\nu' \exp(-E_{ES}/kT)}{FN}\right]^{1/7}, \tag{11}$$

where $(2\pi)^4$ is a geometric prefactor for the circular island and ν' is the attempt frequency of downward hopping, which is assumed the same as the frequency of hopping on terrace in our treatment. Strictly speaking, R_c, the definition of which is given by Eq. (7), is the radius of islands when $(1-1/e)^{-1}$ of them have a new island nucleated on top. The use of Eq. (7) to determine the ES barrier is more suitable when the size distribution of islands is available so that statistical treatment is possible. Our model for the surface morphology assumes that all islands have the same size and they undergo second-layer nucleation at the same time; therefore, there is some degree of ambiguity in determining R_c in our case. Nevertheless, we determine R_c from the size of the first-layer islands at the moment when a nonzero second layer appears. The extracted value of R_c for different RHEED measurement conditions and the ES barrier using Eq. (11) are listed in Table I. For the ES barriers determined from Eq. (11), we find that $\tau_{tr} \ll \tau_{res} \ll \tau_{dep}$ ensuring that they fall in the strong ES barrier limit, justifying the use of Eq. (11) in determining the ES barrier. We notice some scatter among the computed ES barriers using Eq. (11) for various conditions because of the sensitivity of the ES barrier to the value of R_c, the estimated numbers of which exhibit some dispersion. Hence, extremely careful measurements of R_c are required if one is to determine the ES barrier from R_c. In spite of the ambiguity in interpreting the measurement of R_c, as well as some uncertainty of the geometric prefactor in Eq. (11), the average of the ES barriers calculated from Eq. (11) nonetheless is not very off from those obtained from the evolution of layer coverages.

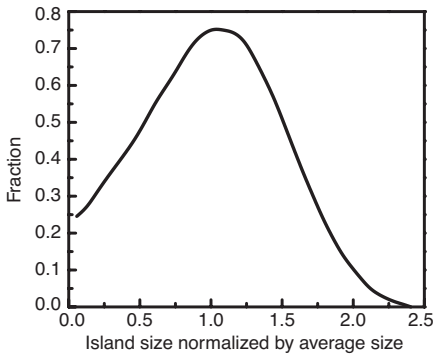

FIG. 7. Island size distribution normalized by average size of islands obtained by KMC simulations with $D/a^4F \sim 10^7$ performed by Amar *et al.*, Ref. 45.

V. DISCUSSION

In applying the model developed above to the measured RHEED intensity, we assumed that the growth surface is composed of circular islands of the same size with a uniform spacing. Now, we relax the assumptions of uniform island size and circular island shape and examine the consequences in the interpretation of RHEED intensity data with regard to the morphological evolution.

There have been extensive studies[44,46,55,64–66] of nucleation and growth of islands during the submonolayer regime of epitaxial growth. Theoretical work on this subject is now well advanced to the stage where the correlation between the size of an island and its capture number is explicitly considered beyond the traditional mean-field treatment,[50] so that it is possible to predict the exact scaling form of island size distributions.[45,65,66] The island size distribution of extended islands (as opposed to point islands) with $D/a^4F \sim 10^7$ from KMC simulations performed by Amar *et al.*[45] is shown in Fig. 7. Although the condition of the simulations ($D/a^4F \sim 10^7$) is different from our experimental condition ($D/a^4F \sim 10^5$), the actual shape varies only weakly[66] with D/a^4F so we consider Fig. 7 representing an actual realistic distribution and use it to obtain the step density. In comparing the step densities evaluated by the realistic size distribution and the uniform size distribution, we find only ~4% difference between them. For example, when the average island radius is 1 nm, the average step density per island turns out to be 6.06 nm using the realistic size distribution and 6.28 nm ($=2\pi \times 1$ nm) using the uniform size distribution. By assuming a uniform island size, we overestimate the step density, which would lead to the underestimation of β or θ_2. However, the magnitude of the underestimate is sufficiently negligible that it should not affect the analysis.

It is well established that like Si(001) surfaces, Ge(001) surfaces also exhibit the (2×1) reconstructions. The asymmetry of (2×1) reconstructions causes the anisotropy of kinetics and energetics of atomic processes and structures on the surface. Diffusion of an ad-dimer on the reconstructed

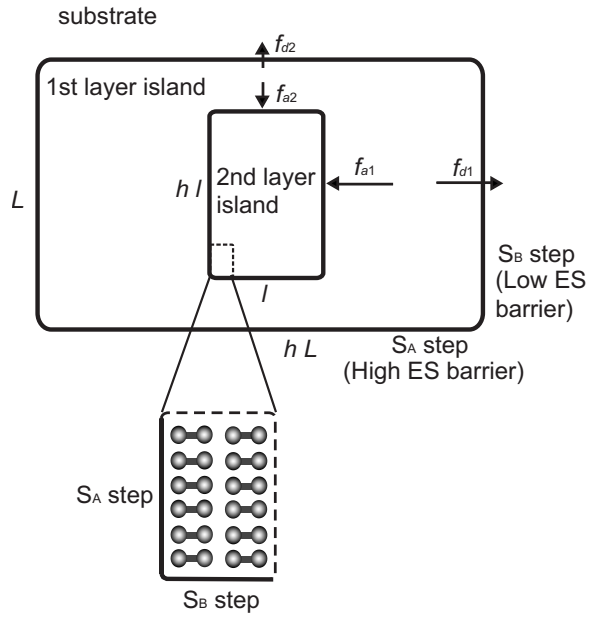

FIG. 8. Schematic of island structure reflecting anisotropic shape. Dumbbell-shaped objects near the bottom of the figure represent dimers. Both first- and second-layer islands are drawn such that they have same aspect ratio h.

surfaces is faster along the underlying dimer row direction and slower perpendicular to the dimer row directions.[42,51,52] The step formation energy has also been shown to be larger for the S_B step (dimer rows on a terrace of higher level perpendicular to the step) than the S_A step (dimer rows parallel to the step),[42,67] as illustrated in Fig. 8. As a result of this anisotropic step formation energy, the submonolayer islands on the Ge(001) surfaces have an anisotropic shape.[49] They are elongated along the direction of the dimer rows so as to have a larger proportion of the lower-energy S_A steps. Dimer rows on adjacent terraces of different levels are aligned perpendicular to each other; hence, the longer direction of a second-layer island is 90° away from that of a first-layer island, as illustrated in Fig. 8. STM studies of the submonolayer growth of Ge(001) homoepitaxy performed by Li *et al.*[49] reveal that the island aspect ratio (h in Fig. 8) is weakly temperature dependent, varying from 2.85 at 140 °C to 2.45 at 270 °C. They also assessed R_c by fitting the exponential form [Eq. (7)] suggested by Tersoff *et al.*[22] to the plots of the fraction of islands with the second-layer nucleation as a function of island size. By comparing R_c and average island spacings in both directions, they concluded that there is no significant barrier for crossing descending S_B steps but a substantial barrier for S_A steps, although no quantitative values for the barrier heights were determined.[49]

As our approach did not include the anisotropy, let us discuss the implication of the anisotropic ES barrier inferred here on our analysis. Considering the anisotropic geometry shown in Fig. 8, the ratio of the flux f_{a1} attaching to the second island to the flux f_{d1} crossing descending steps along the horizontal direction of Fig. 8 is smaller than f_a/f_d of the isotropic case, while f_{a2}/f_{d2} will be larger than f_a/f_d because of the different ES barriers of S_A and S_B steps. Of course, the detailed expressions of f_{a1}/f_{d1} and f_{a2}/f_{d2} will be different from f_a/f_d, which is from the 2D solution of Eq. (8) with axial symmetry and an appropriately averaged effective ES barrier. The one-dimensional (1D) solution of Eq. (8) will be a good approximation for f_{a1}/f_{d1} and f_{a2}/f_{d2}. The ratio of total flux to the second and first islands, Eq. (9), is now modified to $(hlf_{a1}+lf_{a2})/(Lf_{d1}+hLf_{d2})$. The effective ES barrier for the isotropic case is, then, related to the ES barriers of S_A and S_B steps by averaging them in such a way that for a given coverage, the ratio of up and down flux is same for both cases, i.e., $(hf_{a1}+f_{a2})/(f_{d1}+hf_{d2})=f_a/f_b$, where the size of the first-layer island r_1 and the second-layer island r_2 are taken as $h^{0.5}L$ and $h^{0.5}l$.

The ES barrier of Ge(001) surfaces was reported, previously by Van Nostrand *et al.*,[16] to be ~0.045 eV, which is smaller than our best estimate by almost a factor of 2. Their analysis is based on the theory of the instability induced by the ES barrier in the 1D growth developed by Politi and Villain.[14] According to the theory,[14] the onset of instability in homoepitaxy takes place in the absence of a thermal smoothening mechanism at a time of order

$$t^* = \frac{1}{Fa^2}\left(\frac{l_c}{l_{ES}}\right)^2. \tag{12}$$

Here, the nucleation length l_c is defined as the width of a terrace that is just big enough to have a nucleation; it can be considered approximately the same as R_c. By determining l_c and t^*, the ES barrier height can be determined from Eq. (12) via l_{ES}. Because t^* could not be directly determined from their STM analysis, Van Nostrand *et al.*[16] estimated t^* indirectly from the roughening rate as the time when the surface roughness increases by 1 ML. We estimate t^* using their published values of F (0.1 nm/s) (Ref. 68) and the roughening rate (0.75×10^{-3} from Fig. 4 of Ref. 16) to be ~180 ML of deposition of MBE at 155 °C, which seems to be somewhat of an overestimate for the onset of the instability at 155 °C. For example, an STM image of a 70 ML thick MBE film grown at 175 °C [Fig. 1(a) of Ref. 16] already exhibits a well-developed multilayer structure—hence, a yet more pronounced multilayer structure is expected at 155 °C. Clearly, an overestimate of t^* will lead to an underestimate of the ES barrier height. We also note that if we cut t^* by a factor of 2, from 180 ML to 90 ML, the ES barrier height inferred by Van Nostrand *et al.*[16] using Eq. (12) would increase from their reported value of 0.045 eV by ~30% to 0.058 eV: the inferred value of the ES barrier height using Eq. (12) is very sensitive to t^*. Thus, in order to apply Eq. (12) to infer the ES barrier height, one needs a rather precise measurement of t^*, which we find quite challenging. The discrepancy between their value and our value of the barrier height appears to be within the uncertainty of their method. Additionally, they determined l_c from the mean distance between islands on the substrate, which is strictly valid only in the limit of zero or weak ES barrier.[22] Checking the validity of the assumption of zero or weak ES barrier [equivalent to Case I of Ref. 22 or Regime (i) of Ref. 54] in the analysis of Van Nostrand *et al.*[16] by comparing the time scales of atomic processes as explained in Sec. IV C, we find that their reported value of the ES barrier, 0.045 eV, lies in the strong ES

barrier limit, $\tau_{tr} \ll \tau_{res} \ll \tau_{dep}$, contrary to the assumption. For the reasons given above, we believe that our method provides more accurate estimate of the ES barrier height.

Finally, we should comment on the ES barrier height in relation to the kink concentration along step edges. It has been suggested that the kink site offers an easier path for an adatom hopping over downward steps[69] and that the measured ES barrier height should be regarded as an average of the smaller barrier over the kink sites and the larger barrier over straight step edges, weighted by the kink concentration.[28] In this case, the effective ES barrier should be dependent on temperature if the equilibrium kink concentration is achieved—the effective barrier height decreases with increasing temperature due to the increased number of thermally excited kinks on the step edges. However, we find that the ES barriers from 100 to 150 °C (see Table I) lie within the uncertainty of the measurements and analysis because the estimated difference in the kink concentration between 150 and 100 °C is very small.[70] An investigation over a wider range of temperature might provide more insight into this issue.

VI. SUMMARY

In this paper, a model for the RHEED specular intensity in multilayer growth is presented. The model includes the layer interference between terraces of different heights using the kinematic approximation and the diffuse scattering off steps on the surface. We apply our model to the RHEED specular intensity oscillations collected during MBE growth of Ge(001) homoepitaxy at low temperatures, 100–150 °C, with an incident beam angle chosen such that the specular spot is not influenced by Kikuchi features. Under these conditions, RHEED oscillations can be interpreted simply without invoking complicated diffraction calculations. The measured RHEED intensity under various diffraction conditions is well described by the model. We show that the intensity minimum occurs well above 0.5 ML of total deposited coverage, which contradicts the common practice of assigning the intensity minimum to 0.5 ML of deposition.

We apply the model to the submonolayer growth of Ge(001) homoepitaxy by MBE at low temperatures. By fitting the model to the intensity evolution, we find the time-dependent layer coverages. From the evolution of the layer coverages, we infer the effective ES barrier height via the solution of the diffusion equation for adatoms on terraces. We find that in the low temperature Ge(001) homoepitaxy, second-layer nucleation takes place at low coverage, 0.3 ML, implying a substantial ES barrier for this system. A detailed analysis shows that the beam steering effect, which has been neglected so far in the treatment of normal deposition, can affect the estimation of the ES barrier significantly. Including the steering effect, we find a best estimate of the ES barrier height to be 0.084 ± 0.019 eV.

The model for RHEED intensity and the method of inferring the ES barrier height, in principle, can be applied to any system for which RHEED measurements can be obtained without interference from Kikuchi features.

ACKNOWLEDGMENTS

We acknowledge J. P. Leonard for technical assistance and D. G. Cahill for guidance in cleaning Ge. This research was supported by NSF DMR-0306997.

[1] A. Ichimiya and P. I. Cohen, *Reflection High Energy Electron Diffraction* (Cambridge University Press, Cambridge, 2004).
[2] J. J. Harris, B. A. Joyce, and P. J. Dobson, Surf. Sci. **103**, L90 (1981).
[3] E. S. Tok, J. H. Neave, and J. Zhang, Surf. Sci. **515**, 263 (2002).
[4] W. Braun, L. Daweritz, and K. H. Ploog, J. Vac. Sci. Technol. A **16**, 2404 (1998); Phys. Rev. Lett. **80**, 4935 (1998); Z. Mitura, S. L. Dudarev, L. M. Peng, G. Gladyszewski, and M. J. Whelan, J. Cryst. Growth **235**, 79 (2002).
[5] C. S. Lent and P. I. Cohen, Surf. Sci. **139**, 121 (1984); P. R. Pukite, C. S. Lent, and P. I. Cohen, *ibid.* **161**, 39 (1985); G. S. Petrich, P. R. Pukite, A. M. Wowchak, G. J. Whaley, P. I. Cohen, and A. S. Arrott, J. Cryst. Growth **95**, 23 (1989).
[6] P. I. Cohen, P. R. Pukite, J. M. V. Hove, and C. S. Lent, J. Vac. Sci. Technol. A **4**, 1251 (1986).
[7] J. H. Neave, B. A. Joyce, P. J. Dobson, and N. Norton, Appl. Phys. A: Solids Surf. **31**, 1 (1983); J. H. Neave, P. J. Dobson, B. A. Joyce, and J. Zhang, Appl. Phys. Lett. **47**, 100 (1985); S. Clarke and D. D. Vvedensky, Phys. Rev. B **37**, 6559 (1988); T. Shitara, D. D. Vvendensky, and M. R. Wilby, *ibid.* **46**, 6815 (1992).
[8] J. Sudijono, M. D. Johnson, C. W. Snyder, M. B. Elowitz, and B. G. Orr, Phys. Rev. Lett. **69**, 2811 (1992).
[9] D. M. Holmes, J. L. Sudijono, C. F. McConville, T. S. Jones, and B. A. Joyce, Surf. Sci. **370**, L173 (1997).
[10] Z. Mitura, S. L. Dudarev, and M. J. Whelan, Phys. Rev. B **57**, 6309 (1998).
[11] J. Zhang, J. H. Neave, P. J. Dobson, and B. A. Joyce, Appl. Phys. A: Solids Surf. **42**, 317 (1987); K. Nemcsics, Thin Solid Films **412**, 60 (2002); J. Resh, K. D. Jamison, J. Strozier, A. Bensaoula, and A. Ignatiev, Phys. Rev. B **40**, 11799 (1989).
[12] B. Shin, J. P. Leonard, J. W. McCamy, and M. J. Aziz, J. Vac. Sci. Technol. A **25**, 221 (2007).
[13] J. Villain, J. Phys. I **1**, 19 (1991).
[14] P. Politi and J. Villain, Phys. Rev. B **54**, 5114 (1996).
[15] N. E. Lee, G. Xue, and J. E. Greene, J. Appl. Phys. **80**, 769 (1996).
[16] J. E. Van Nostrand, S. J. Chey, and D. G. Cahill, Phys. Rev. B **57**, 12536 (1998).
[17] K. A. Bratland, Y. L. Foo, J. Soares, T. Spila, P. Desjardins, and J. E. Greene, Phys. Rev. B **67**, 125322 (2003).
[18] M. D. Johnson, C. Orme, A. W. Hunt, D. Graff, J. Sudijono, L. M. Sander, and B. G. Orr, Phys. Rev. Lett. **72**, 116 (1994).
[19] K. Thurmer, R. Koch, M. Weber, and K. H. Rieder, Phys. Rev. Lett. **75**, 1767 (1995).
[20] K. Bromann, H. Brune, H. Roder, and K. Kern, Phys. Rev. Lett. **75**, 677 (1995).
[21] K. Morgenstern, G. Rosenfeld, E. Laegsgaard, F. Besenbacher,

and G. Comsa, Phys. Rev. Lett. **80**, 556 (1998).
[22] J. Tersoff, A. W. Denier van der Gon, and R. M. Tromp, Phys. Rev. Lett. **72**, 266 (1994).
[23] P. Smilauer and S. Harris, Phys. Rev. B **51**, 14798 (1995).
[24] J. A. Meyer, J. Vrijmoeth, H. A. Vandervegt, E. Vlieg, and R. J. Behm, Phys. Rev. B **51**, 14790 (1995).
[25] I. Markov, Phys. Rev. B **54**, 17930 (1996).
[26] S. Harris, Phys. Rev. B **53**, 7500 (1996).
[27] J. Krug, P. Politi, and T. Michely, Phys. Rev. B **61**, 14037 (2000).
[28] P. Politi and C. Castellano, Phys. Rev. B **67**, 075408 (2003).
[29] R. Gerlach, T. Maroutian, L. Douillard, D. Martinotti, and H. J. Ernst, Surf. Sci. **480**, 97 (2001).
[30] K. R. Roos and M. C. Tringides, Phys. Rev. Lett. **85**, 1480 (2000).
[31] J. G. Amar, Phys. Rev. B **52**, 13801 (1995).
[32] S. Kodiyalam, K. E. Khor, and S. Das Sarma, Phys. Rev. B **53**, 9913 (1996).
[33] I. Markov, Phys. Rev. B **50**, 11271 (1994).
[34] M. Kalff, G. Comsa, and T. Michely, Phys. Rev. Lett. **81**, 1255 (1998).
[35] F. Tsui, J. Wellman, C. Uher, and R. Clarke, Phys. Rev. Lett. **76**, 3164 (1996).
[36] By "submonolayer," we include the regime in which the total coverage is <1 ML but the coverage is distributed among multiple layers.
[37] ksa 400 from k-Space Associates, Inc.
[38] B. Shin, J. P. Leonard, J. W. McCamy, and M. J. Aziz, Appl. Phys. Lett. **87**, 181916 (2005).
[39] D. H. A. Blank, G. Koster, G. A. J. H. M. Rijnders, E. van Setten, P. Slycke, and H. Rogalla, J. Cryst. Growth **211**, 98 (2000).
[40] U. Korte and P. A. Maksym, Phys. Rev. Lett. **78**, 2381 (1997).
[41] G. R. Bell, T. S. Jones, J. H. Neave, and B. A. Joyce, Surf. Sci. **458**, 247 (2000).
[42] H. J. W. Zandvliet, Phys. Rev. B **61**, 9972 (2000).
[43] G. Lehmpfuhl, A. Ichimiya, and H. Nakahara, Surf. Sci. **245**, L159 (1991).
[44] G. S. Bales and D. C. Chrzan, Phys. Rev. B **50**, 6057 (1994).
[45] J. G. Amar, M. N. Popescu, and F. Family, Surf. Sci. **491**, 239 (2001).
[46] H. Brune, G. S. Bales, J. Jacobsen, C. Boragno, and K. Kern, Phys. Rev. B **60**, 5991 (1999).
[47] G. T. Barkema, O. Biham, M. Breeman, D. O. Boerma, and G. Vidali, Surf. Sci. **306**, L569 (1994).
[48] The distributions of the total coverage, 1.15 ML, are $\theta_1 \sim 1/(1+0.35) \sim 0.85$ ML and $\theta_2 \sim 0.35$ ML with $k \sim 0.35$, for example.
[49] M. Li and E. I. Altman, Surf. Sci. **526**, L117 (2003).
[50] J. A. Venables, G. D. T. Spiller, and M. Hanbucken, Rep. Prog. Phys. **47**, 399 (1984).
[51] T. V. Afanasieva, S. Y. Bulavenko, I. F. Koval, and H. J. W. Zandvliet, J. Appl. Phys. **93**, 1452 (2003).
[52] H. J. W. Zandvliet, T. M. Galea, E. Zoethout, and B. Poelsema, Phys. Rev. Lett. **84**, 1523 (2000).
[53] J. Rottler and P. Maass, Phys. Rev. Lett. **83**, 3490 (1999).
[54] P. Politi and C. Castellano, Phys. Rev. E **66**, 031605 (2002).
[55] P. Politi and C. Castellano, Phys. Rev. E **66**, 031606 (2002).
[56] As we consider ad-dimer as a unit entity on the surface, the hopping distance here is taken as the average of the distance between ad-dimers along dimer rows, ~0.4 nm, and perpendicular to dimer rows, ~0.8 nm.
[57] G. H. Vineyard, J. Phys. Chem. Solids **3**, 121 (1957).
[58] Another common type of the boundary conditions used in this type of diffusion problem is the so-called "absorbing" boundary conditions (see Ref. 29, for example). However, it was shown by Harris (Ref. 26) that the absorbing boundary conditions lead to the inconsistency of an initial growth law of an island between exact solution and steady-state solution.
[59] J. Krug, Phys. Rev. Lett. **87**, 149601 (2001); K. R. Roos and M. C. Tringides, *ibid.* **87**, 149602 (2001); K. Morgenstern and F. Besenbacher, *ibid.* **87**, 149603 (2001); K. R. Roos and M. C. Tringides, *ibid.* **87**, 149604 (2001); S. Heinrichs and P. Maass, *ibid.* **87**, 149605 (2001); K. R. Roos and M. C. Tringides, *ibid.* **87**, 149606 (2001).
[60] D. E. Sanders, D. M. Halstead, and A. E. Depristo, J. Vac. Sci. Technol. A **10**, 1986 (1992).
[61] S. van Dijken, L. C. Jorritsma, and B. Poelsema, Phys. Rev. B **61**, 14047 (2000); J. Seo, H. Y. Kim, and J. S. Kim, *ibid.* **71**, 075414 (2005).
[62] See Fig. 6 of Ref. 28.
[63] The original definition is a $(D/D'-1)$, where D' is the rate of interlayer transport. Assuming that the attempt frequency for D and D' is the same, it becomes $a[\exp(E_{ES}/kT)-1]$.
[64] C. Ratsch and J. A. Venables, J. Vac. Sci. Technol. A **21**, S96 (2003).
[65] P. A. Mulheran, Europhys. Lett. **65**, 379 (2004); J. W. Evans and M. C. Bartelt, Phys. Rev. B **66**, 235410 (2002); M. C. Bartelt, C. R. Stoldt, C. J. Jenks, P. A. Thiel, and J. W. Evans, *ibid.* **59**, 3125 (1999); J. G. Amar and M. N. Popescu, *ibid.* **69**, 033401 (2004); J. G. Amar, M. N. Popescu, and F. Family, Phys. Rev. Lett. **86**, 3092 (2001).
[66] M. C. Bartelt and J. W. Evans, Phys. Rev. B **54**, 359 (1996).
[67] C. Tegenkamp, J. Wollschlager, H. Pfnur, F. Heringdorf, and M. Horn-von Hoegen, Phys. Rev. B **65**, 235316 (2002).
[68] J. E. Van Nostrand, S. J. Chey, M.-A. Hasan, D. G. Cahill, and J. E. Greene, Phys. Rev. Lett. **74**, 1127 (1995).
[69] R. Kunkel, B. Poelsema, L. K. Verheij, and G. Comsa, Phys. Rev. Lett. **65**, 733 (1990); M. Bott, T. Michely, and G. Comsa, Surf. Sci. **272**, 161 (1992); P. Smilauer, M. R. Wilby, and D. D. Vvedensky, Phys. Rev. B **47**, 4119 (1993).
[70] Using the literature values of kink formation energy at S_A and S_B steps on Ge(001) surfaces from Ref. 42, we estimate the kink concentration along S_A (S_B) step at 150 and 100 °C as 0.06 (0.32) and 0.04 (0.28), respectively.